Geophysical Research Letters

RESEARCH LETTER
10.1029/2021GL092988

Key Points:

- First direct observation of an intermediate nepheloid layer in the Eurasian part of the Arctic Ocean
- Coinciding strong midwater turbulence is likely caused by a down-slope current displacing isopycnals
- Similar downslope flow events exhibit a strong seasonality toward the ice free season

Correspondence to:
K. Schulz,
kirstin.schulz@awi.de

Citation:
Schulz, K., Büttner, S., Rogge, A., Janout, M., Hölemann, J., & Rippeth, T. P. (2021). Turbulent mixing and the formation of an intermediate nepheloid layer above the Siberian continental shelf break. *Geophysical Research Letters*, *48*, e2021GL092988. https://doi.org/10.1029/2021GL092988

Received 15 FEB 2021
Accepted 14 APR 2021

Turbulent Mixing and the Formation of an Intermediate Nepheloid Layer Above the Siberian Continental Shelf Break

Kirstin Schulz[1], Stefan Büttner[2], Andreas Rogge[1,2], Markus Janout[1], Jens Hölemann[1], and Tom P. Rippeth[3]

[1]Alfred Wegener Institute, Helmholtz Centre for Polar and Marine Research, Bremerhaven, Germany, [2]Institute for Ecosystem Research, Christian Albrechts University Kiel, Kiel, Germany, [3]School of Ocean Sciences, Bangor University, Bangor, UK

Abstract Intermediate nepheloid layers (INLs) form important pathways for the cross-slope transport and vertical export of particulate matter, including carbon. While intermediate maxima in particle settling fluxes have been reported in the Eurasian Basin of the Arctic Ocean, direct observations of turbid INLs above the continental slope are still lacking. In this study, we provide the first direct evidence of an INL, coinciding with enhanced mid-water turbulent dissipation rates, over the Laptev Sea continental slope in summer 2018. Current velocity data show a period of enhanced downslope flow with depressed isopcynals, suggesting that the enhanced turbulent dissipation is probably the consequence of the presence of an unsteady lee wave. Similar events occur mostly during ice free periods, suggesting an increasing frequency of episodic cross-slope particle transport in the future. The discovery of the INL and the episodic generation mechanism provide new insights into particle transport dynamics in this rapidly changing environment.

Plain Language Summary In the Arctic Ocean deep basins, only a tiny fraction of the algae that grows in the surface layer sinks down to the sea floor. Most of the particles reaching the sea floor originate from the shallower regions closer to the coast. These particles have already settled on the sea floor once, and originate from rivers or algae that grew, died and sank down in shallow regions. Later, these particles are lifted off the ground again by strong turbulent motions and transported toward deeper regions in the middle of the water column. These lift-off and transport events happen only occasionally, and have not been directly observed in the Eurasian part of the Arctic Ocean yet. Also, we present a new mechanism for the creation of turbulence, which is necessary to lift particles off the sea floor. This mechanism happens mostly during the summer season, when less sea ice is present. Based on this seasonality, it is likely that sediment transport events will become more frequent in the future, when the Arctic sea ice is further declining.

1. Introduction

Particle transport pathways and organic carbon cycling in the Arctic Ocean are substantially different compared to the rest of the world's pelagic oceans (Hwang et al., 2008; Honjo et al., 2010). The vertical export of surface primary production particulate organic matter by gravitational sinking and migrating zooplankton is inefficient (Honjo et al., 2010), and only contributes to 1%–2% of the interior basin particulate organic carbon (POC) supply (Hwang et al., 2015). Particle and POC settling fluxes are strongly affected by sea ice melt, via the deposition of large under-ice algae biomass (Boetius et al., 2013), and the release of sediments from dirty sea ice (e.g., Krumpen et al., 2019). Both processes are episodic in time and are becoming increasingly important in the central Arctic Ocean due to intensified melt. In the vicinity of the basin margins, particle fluxes are dominated by lateral advection of resuspended lithogenic ballasted material from the continental slopes (Fahl & Nöthig, 2007; Forest et al., 2015, 2016; Honjo et al., 2010; Hwang et al., 2008, 2015; Osborne & Forest, 2016; Xiang & Lam, 2020). This principal transport pathway closely links the basin interior and the disproportionately large shelf sea areas of the Arctic. Anticipated changes in the near coastal areas, like increased anthropogenic use or thawing permafrost — therefore have the potential to impact the entire Arctic Ocean. Resolving the transport mechanisms connecting the Arctic shelf and interior basin is hence a key

issue to understand organic carbon cycling and particle transport pathways (Forest et al., 2015), especially in the light of a rapidly changing Arctic system, which will likely impact particle sources and transport (Xiang & Lam, 2020).

Isopycnal intrusions of detached bottom nepheloid layers, forming intermediate nepheloid layers (INLs), may initiate the basin-ward transport of resuspended particles from the continental margin (Hwang et al., 2008). INLs have been observed in the vicinity of continental margins at lower latitudes (Azetsu-Scott et al., 1995; Cacchione & Drake, 1986; de Madron et al., 1990, 1999; Gardner & Walsh, 1990; Pak et al., 1980; Puig & Palanques, 1998; Thorpe & White, 1988; van Weering et al., 2001), where the turbid bottom layer is detached from the topographic slope and spreads seaward (McPhee-Shaw et al., 2004). These INLs form important pathways for the transport of particles including carbon, nutrients, and lithogenic material from the shelf to the deep ocean (McCave & Hall, 2002; McPhee-Shaw et al., 2004; van Weering et al., 2001) and can thus contribute to the long-term sequestration of carbon in the ocean (McPhee-Shaw, 2006) and affect the deep-water benthic population structure (Puig et al., 2001). Most INLs are linked to enhanced turbulent mixing often associated with breaking of an internal tide (Azetsu-Scott et al., 1995; Cacchione & Drake, 1986; de Madron et al., 1999; Dickson & McCave, 1986; McPhee-Shaw et al., 2004; Thorpe & White, 1988). In the Arctic Ocean, however, most continental slope regions are located poleward of the critical latitude for the generation of a freely propagating linear internal tide, but the generation of an unsteady lee-wave can result in significant turbulent mixing (Fer et al., 2015, 2020; Rippeth et al., 2017).

The existence of INLs and their importance for seaward particle fluxes in the Amerasian part of the Arctic Ocean was first suspected by O'Brien et al. (2006), over the slope of the Mackenzie shelf in the Canadian Beaufort Sea, and later confirmed by Forest et al. (2007). Strong atmospheric cooling, ice formation and the resulting thermohaline convection provide a mechanism for shelf sediment resuspension and advection at high latitudes, explaining the observed dominant contribution of resuspended material to the vertical POC flux over the Mackenzie shelf slope in fall and winter (Forest et al., 2007). Mesoscale eddies are suspected to further amplify basin-ward transport of turbid waters originating from the shelf and upper slope regions (Forest et al., 2007, 2015; Osborne & Forest, 2016). Furthermore, large scale wind dynamics inducing downwelling (Osborne & Forest, 2016) and resuspension by surges of fast barotropic currents (Forest et al., 2016) were found to facilitate shelf-basin particle transport in the Canadian Beaufort Sea.

Observations of INLs in the Eurasian Arctic Ocean are, however, extremely scarce. Fahl and Nöthig (2007) found high vertical fluxes of mostly lithogenic material at intermediate depths above the southern Lomonosov Ridge, presumably caused by lateral advection from the Laptev Sea continental margin. Xiang and Lam (2020) report intermediate lithogenic particle maxima in the Arctic basins, with elevated concentrations on the Eurasian side of the Lomonosov Ridge, and suspect dense-water cascading in winter as the major lateral transport process. Evidence of a turbid INL was observed over the Laptev Sea inner shelf (water depths < 60 m), probably caused by a displacement of the bottom nepheloid layer in the vicinity of a shallow bank (Wegner et al., 2003). Even though the Siberian continental slope region is frequently sampled since the early 2000s in the context of the NABOS (Nansen and Amundsen Basins Observational System), and more recently the CATS (Changing Arctic Transpolar System) project, to the authors knowledge no direct observations of turbid INLs have been reported in this region, or anywhere at latitudes polewards of the critical M2-latitude at 74.5°N.

Here, we provide the first evidence of the presence of intermittent INLs over the continental shelf break of the Laptev Sea. The evidence is based on vertical profiles of particulate matter concentration, size distribution, and carbon content, and contemporaneous turbulent microstructure measurements, taken during an ice-free period in the summer of 2018. Coincident velocity measurements provide clues as to the episodic generation mechanism and suggest it is seasonal in nature.

2. Data and Methods

From August 18 to September 29, 2018, the continental shelf break region of the Laptev and East Siberian Sea, between 92°E and 160°E, was sampled during an expedition with the *Akademik Tryoshnikov*. In total, 11 cross-slope transects were performed, distributed over an approximately 2,500 km distance along the shelf break. In the following, we will mainly present data from one transect in the central Laptev Sea,

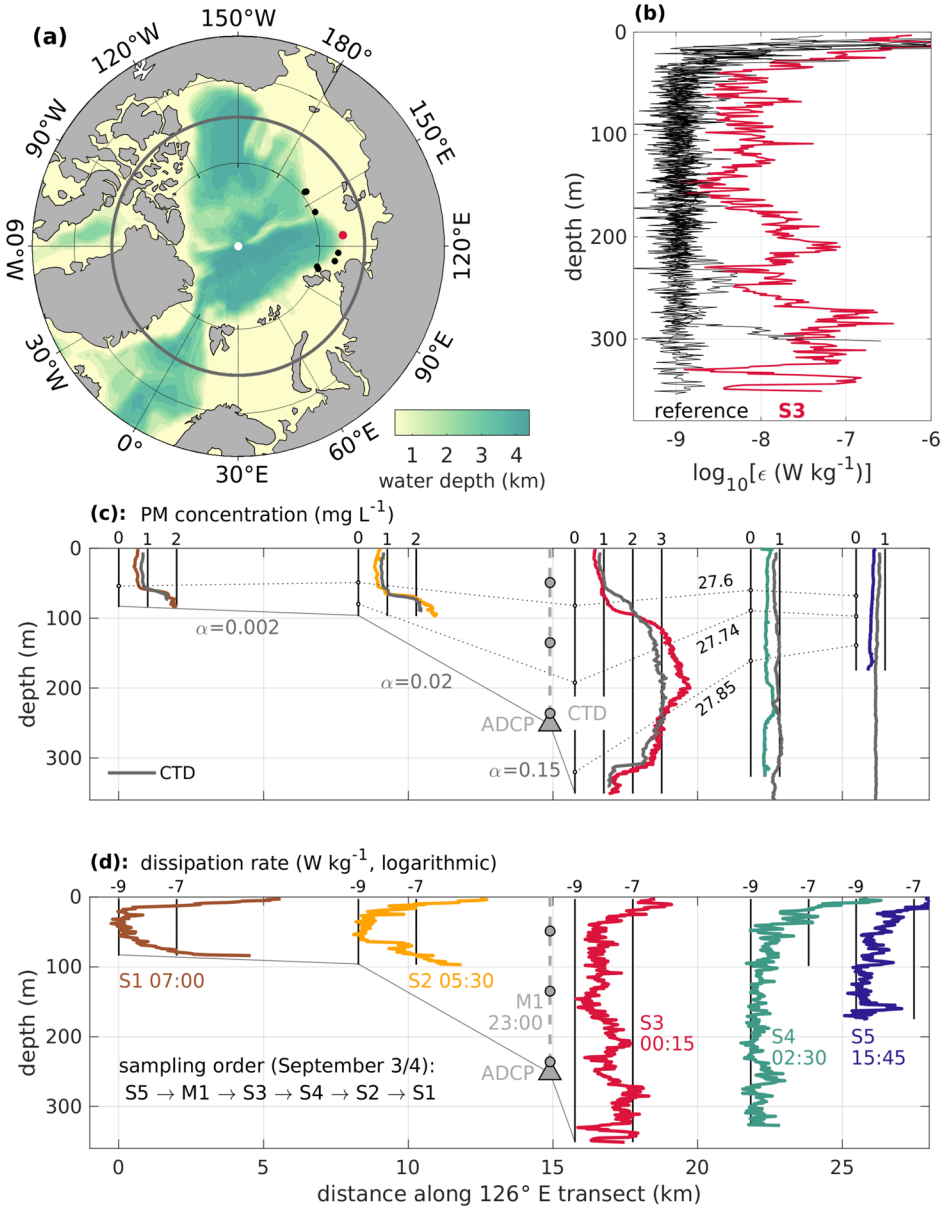

Figure 1. (a) Map of the Arctic Ocean, with the critical M_2 latitude (gray line) and the position of the INL (red dot) and reference stations (black dots) indicated, (b) vertical profiles of turbulent dissipation rate (W kg^{-1}) at station S3 (red) and the reference stations (black). Vertical profiles of (c) PM concentration (mg L^{-1}, measurement position at the vertical 0 line) and (d) turbulent dissipation rate (W kg^{-1}, measurement position at the vertical −9 line), measured along the cross-slope transect at 126°E. In (c), colored lines indicate data from the microstructure profiler, gray lines refer to CTD profiles at the same position, isopycnals are indicated with dotted black lines. The dashed gray line in (c) and (d) indicates the position of the mooring chain with the ADCP (triangle) and CTDs (circles). ADCP, Acoustic Dopper Current Profiler; CTD, conductivity, temperature, depth.

at 77°N, 126°E (see Tarasenko et al., 2021, Schulz et al., 2021, and Figure 1 for details). At each station, ship-based conductivity, temperature, depth (CTD) casts were carried out, along with 2–3 consecutive casts with a microstructure (MSS) profiler, equipped with shear probes to estimate turbulent dissipation rates. Depending on the water depth, one MSS casts took around 10–20 min, the 2–3 performed MSS casts were subsequently averaged to obtain one mean profile per station. Both CTD and MSS were equipped with an optical backscatter (OBS) turbidity sensor, which was calibrated with 166 in-situ water filtration samples for total particulate matter (PM) concentration (PM (mg L^{-1}) = 1.88 × OBS (NTU) + 0.61, R^2 = 0.82). For each

PM sample, a water volume of 1–2 L was filtered through pre-weighed MILLIPORE filters with a diameter of 47 mm and a pore size of 0.45 μm, and dried for 24 h at 60°C directly after sampling and again before weighing in the laboratory.

An Underwater Vision Profiler 5hd (UVP, Hydroptic) was mounted inside the CTD frame to obtain profiles of particle abundances and their size distribution. Sampling frequency of the UVP was 20 Hz, the sampling volume was approximately 1 L. Post-processing of the large particulate matter data and vignettes was accomplished using the ImageJ based software Zooprocess (Gorsky et al., 2010).

In addition, 92 size fractionated POC samples were taken. Fine particles <100 μm (sample volume 1–2 L) were filtered over a 100 μm MILLIPORE nylon mesh and subsequently onto 0.8 μm GFF filters (Whatman), dried and stored at −80°C until acidification in the laboratory to remove carbonates. An element analyzer (Euro EA Elemental Analyzer, Model: EURO EA 3000, EUROVECTOR S.p.A., Via Tortona 5) was used to quantify carbon content of the tin encapsulated samples. Excluding fluorescent data points near the surface, POC data were related to turbidity values from the OBS sensor on the CTD. A Theil-Sen regression, which is less sensitive to the many outliers in the data (Sprent, 2012), was used to obtain the linear regression $POC_{<100\,\mu m}$ (mol L^{-1}) = $2.62 \times 10^{-6} \times$ OBS (NTU) + 6.93×10^{-7}. POC data for the fraction of large particles >100 μm (the UVP size range, sample volume 20–60 L), exhibited no sufficient correlation to the volumetric particle concentration measured with the UVP. Hence, we only use the particle size distribution data from the UVP, and do not estimate POC content in the large particle fraction. Consequently, POC values in this study refer to POC in particles <100 μm and are likely an underestimation of the total POC content.

Furthermore, a mooring line consisting of an upward-looking 75 kHz Acoustic Dopper Current Profiler (ADCP) (Workhorse Sentinel, Teledyne RD Instruments), profiling the water column between 40 and 230 m in 5 m bins at hourly resolution, and three CTDs (SBE37, Sea-Bird Scientific, temporal resolution of 15 min) at 49, 135, and 236 m water depth was deployed on the transect in September 2015 and recovered during the transect measurements. Only data from the lowermost two CTDs were used in this study, as the shallowest CTD was affected by tilt on the mooring line in the presence of strong currents. The acoustic backscatter data of the ADCP was not suited to describe PM concentration, we suspect that the majority of suspended particles were too small to reflect the 75 kHz acoustic signal. Details on the instrumentation, data processing and sampling procedures can be found in Schulz et al. (2021) (MSS and CTD) and Polyakov, Rippeth, Fer, Alkire, et al. (2020); Polyakov, Rippeth, Fer, Baumann, et al. (2020) (ADCP).

3. Results

3.1. Particle Distribution and Turbulent Mixing

At station S3, located at approximately 360 m water depth at the Laptev Sea continental slope, we observed an intermediate water layer characterized by unusually high PM concentrations, along with strongly enhanced turbulent dissipation rates over the whole water column (Figure 1). The integrated PM concentration in this INL (60–310 m) is approximately 650 g m^{-2}, the integrated POC content is 10 g m^{-2}. No comparable turbid and turbulent layer was found on any of the other ten cross-slope transects performed during the expedition. Mid-water turbulent dissipation rates at S3 are up to 10^{-7} W kg^{-1}, two orders of magnitude higher than the values of 10^{-9} W kg^{-1} typically observed in intermediate water layers above the continental slope (based on stations measured at water depths between 250 and 600 m on other transect during the same expedition, see Figures 1a and 1b).

Already less than 10 km further offshore, at station S4, no enhanced PM concentrations or strongly enhanced turbulence at intermediate layers are present. At the two shallower shelf stations on this transect (S1 and S2, Figure 1), a frictional turbid bottom boundary layer with a vertical extent of 25 m (S1) to 35 m (S2) is found. PM concentrations there are higher than typically found in the near bottom layer at other shelf stations during the same measurement campaign, but much lower than the mid-water maximum PM concentration at station S3 (Figure 2c). This PM distribution points to a source of turbidity further downslope, between S2 and S3, rather than on the shelf.

The INL at S3 is characterized by a potential density anomaly of $\sigma_\theta = 27.74$ kg m^{-3}, corresponding to the density of the near bottom waters at S2 (Figures 2a and 2b). Together with the similar particle size distribution

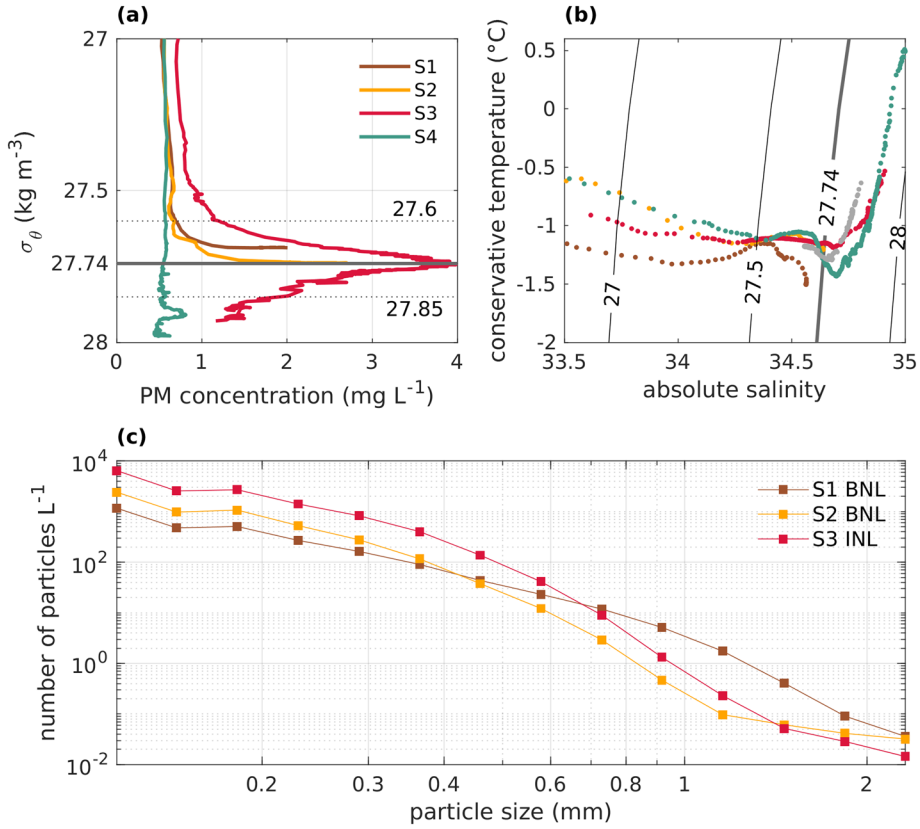

Figure 2. (a) Vertical profiles of PM concentration, displayed against density for stations S1–S4, and (b) the corresponding T-S diagrams. In (b), gray dots show a time series of the T-S data from the near-bottom moored CTD at M1 prior to recovery (second gray patch in Figure 3). (c) Number of particles per particle size class at stations S1–S3, recorded with the UVP. CTD, conductivity, temperature, depth; PM, particulate matter; UVP, Underwater Vision Profiler.

(PSD) observed in both layers (Figure 2c), at least in the range of particles smaller than 1.29 mm, these similar water mass properties point to a common origin of the encountered high PM concentrations. Again, the total amount of (small) particles encountered in the INL at S3 is on average 3 times higher than in the near bottom layer at S2. The near bottom water properties and PSD at S1, however, differ from those at S2 and S3: The water is colder, less saline, and characterized by a lower density of $\sigma_\theta = 27.69$ kg m^{-3}. Only particles smaller than 0.323 mm exhibit the same size class distribution at S1, compared to S2 and S3. In contrast, large particles exhibit a trend toward higher concentrations at the shallower shelf stations. This station is still some 100 km away from any riverine input, hence the large particles might be locally resuspended (i.e., the bottom sediment composition is different compared to the origin of the INL) or were transport up-slope within the bottom boundary layer (Schulz et al., 2017; Schulz & Umlauf, 2016).

3.2. Flow Regime

Current velocities, measured with the ADCP moored at M2, generally exhibit a flow to the east, roughly aligned with the isobaths, and associated with with the Arctic Circumpolar Current transporting Atlantic Water along the Arctic Basin margins, superimposed with weak ($\mathcal{O}(0.1)$ m s^{-1}), mainly barotropic semidiurnal tidal motions. Current velocities are generally smaller and less variable between February and June, compared to the time between July and January. While the transect profiles were measured, a period of intensified current velocities over the whole water column occurred, with maximum depth-averaged velocities over 0.5 m s^{-1}, lasting for at least 24 h (event II, Figure 3b). A similar event with intensified current velocities over a period of approximately 48 h was recorded 4 days earlier (event I, Figure 3b). During both events, the flow was mainly directed along-slope (eastward), but with a significant down-slope (northward)

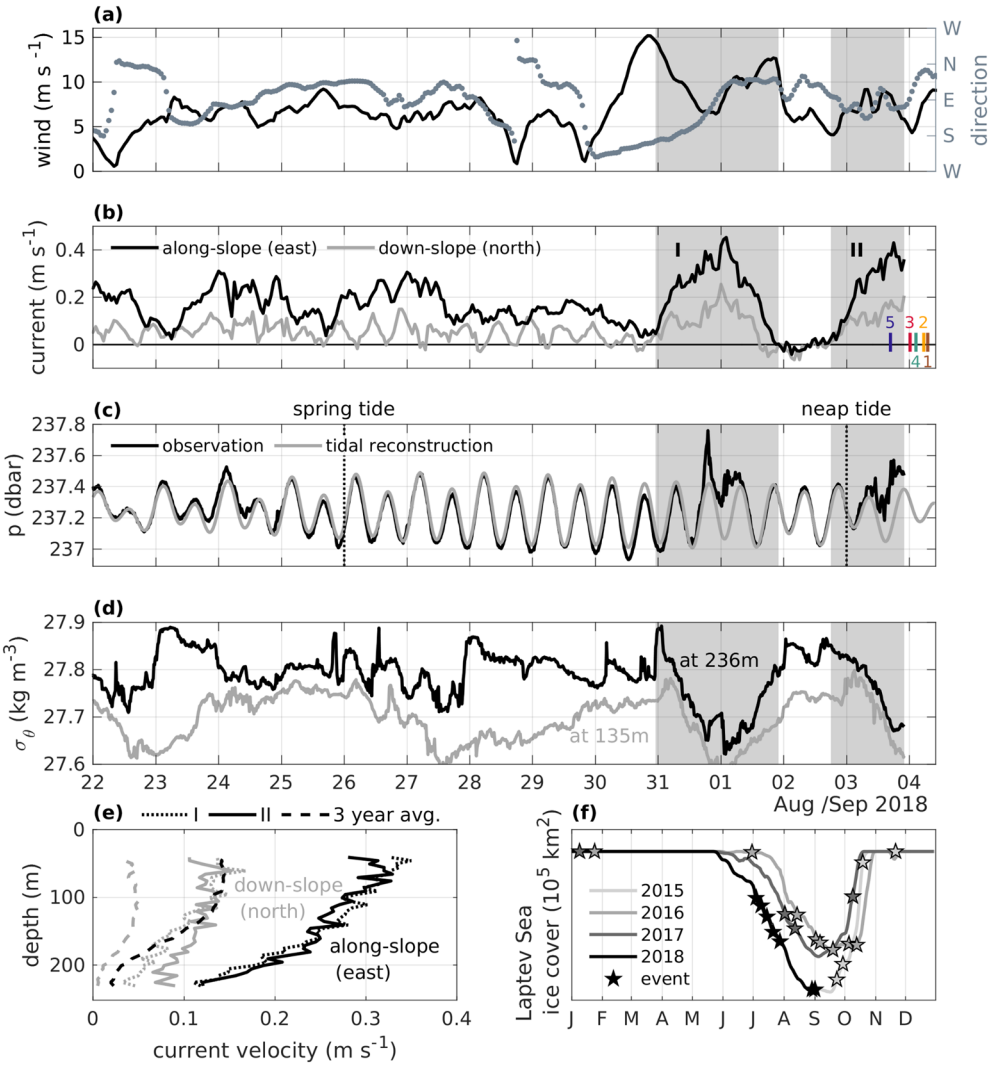

Figure 3. Time series of (a) wind speed (left vertical axis) and direction (right vertical axis), (b) depth-averaged current velocity in east (black line) and north (gray line) direction recorded with the moored ADCP at M1, (c) measured pressure (black line) and tidal reconstruction (gray line), and (d) density anomaly recorded with two CTDs at the M1 mooring (see Figure 1). Colored lines in (b) indicate the time of the respective water column stations. (e) Vertical profiles of the current velocity in east (black lines) and north (gray line) direction, averaged over the duration of event I (dotted lines), event II (solid lines) and the 3-year deployment period (dashed lines). (f) Time series of Laptev Sea sea ice cover (km^2), color-coded by year, with events (down-slope velocity > 0.15 m s^{-1}, $\Delta\sigma_\theta$ > 0.15 kg m^{-3}) indicated with stars. ADCP, Acoustic Dopper Current Profiler; CTD, conductivity, temperature, depth.

component with a depth-averaged maximum current speed over 0.2 m s^{-1}. While variations in sea surface height (black line, Figure 3c) are mostly caused by tides (gray line, Figure 3c, tidal reconstruction based on the full 3-year time series, using the UTide Matlab toolbox (Codiga, 2011)) and pressure data from the lowermost CTD, positive pressure anomalies were recorded during both events.

Furthermore, a decrease of both water temperature and salinity, resulting in a decrease in potential density of over 0.2 kg m^{-3} within 24 h, indicates a strong downward displacement of isopycnals (Figure 3d). The corresponding vertical isopycnal displacement was at least larger than the 100 m distance between the moored CTDs (see Figure 3d). The minimum density anomaly recorded during both events in the lowermost CTD, 27.7 kg m^{-3}, was found at a depth of approximately 70 m at the shelf station S2, suggesting that the vertical displacement was probably even larger than 150 m.

The vertical structure of the time-averaged current profiles during the two events (gray patches in Figure 3) is very similar (Figure 3e). Current velocities are vertically rather homogeneous in the upper 80–140 m, around 0.3 m s^{-3} in eastward and 0.1 m s^{-1} in northward (downslope) direction, and current velocities decrease toward the bottom. In particular, the eastward flow component exhibits strong shear in the deeper layers.

4. Discussion

4.1. Origin of the Turbid Layer

No similar INLs have been observed on the other 10 transects measured during the expedition, hence there is no indication for the along-slope advection of material originating from upstream of the boundary current. The down-slope transport of PM in the near bottom layer from the shallower continental shelf region as a dense gravity current, and the subsequent detachment of this turbid layer near the shelf break, would result in a cross-slope PM concentration gradient from high PM concentration at the upper shelf to lower concentrations at the shelf break, opposite to the observed situation (Figure 2a) and is, hence, also unlikely. Furthermore, the strongly enhanced dissipation rates encountered at S3 point toward local resuspension, and a subsequent detachment and offslope transport of the turbid near bottom layer. The similar PSD and water mass properties in the INL at S3 and the BNL at S2 (Figure 2c) further indicate that both turbid layers have a common origin.

INLs are often characterized by uniform temperature and salinity properties (Thorpe & White, 1988), which are associated with the water mass properties of the turbid near-bottom layer from which they originate (Moum et al., 2002). While the density of the turbid water mass observed over the slope is similar to the density of the near bottom layer at the 94 m deep shelf station S2 (Figure 2a), both the observed temperature and salinity are slightly higher, by 0.04°C and 0.03, respectively, indicating that the observed intermediate PM concentration maximum originates from a slightly deeper position than S2. Hence, the formation of the observed INL at S3 and the enhanced PM concentration in the near bottom layer at S2 can be conclusively explained by strong mixing and local resuspension at the upper continental slope, and the subsequent detachment and spreading of the turbid layer.

The question remains how the strong turbulence was generated. Frictional effects alone are unlikely, as bottom boundary layers are typically confined to a few 10 m thickness, and are characterized by suspended PM concentrations that increase toward the bottom. A storm event with wind speeds up to 15 m s^{-1} and a change in wind direction from toward south-westerly to north-easterly directions took place on August 30, but the winds decayed again shortly after (Figure 3a). During the measurements, 4 days later, winds were steady toward the north-east with speeds between 5 and 10 m s^{-1}. However, wind-driven mixing is confined to the surface layer, even during a storm event, and is unlikely to induce strongly enhanced dissipation at depths of over 300 m. Moreover, local barotropic tidal currents and local tidal conversion (Rippeth et al., 2015) in this region are weak.

We find the enhanced mid-water dissipation to coincide with a period of significant down-slope barotropic flow and a depression in the isopcynals (Figures 3b and 3d). In other continental slope regions in the Arctic, observed strong mid-water dissipation was found to be associated with unsteady lee waves generated by a cross-isobath tidal current (Padman et al., 1992; Rippeth et al., 2017; Fer et al., 2015, 2020). Based on an extensive observational data set including a 24 h time series of temperature, salinity, dissipation rate and current velocity profiles, Fer et al. (2020) report enhanced mid-water turbulence over a period of 6 h, following the downslope flow phase of a diurnal tidal current above Yermak Plateau. The topographic setting (slope and water depth), and the magnitude of the downslope velocity discussed here are comparable to the situation described in Fer et al. (2020). Whilst in the case presented here the off-shelf barotropic flow is not the result of a tide, which is weak in this region, the period of the downslope flow (~2 days, see Figure 3b) is longer than the local inertial period at this latitude, and so the lee wave generated by the downslope barotropic flow will be bottom trapped (Fer et al., 2015; Rippeth et al., 2017). As such we identify the unsteady lee-wave mechanism, proposed for dissipation of the tide over the shelf breaks poleward of the critical latitude (e.g., Fer et al., 2020; Rippeth et al., 2017), as potentially supporting the observed enhanced mid-water dissipation.

4.2. Spatial and Temporal Distribution of INLs

Two events of enhanced (downslope) current velocities and downward isopycnal displacement were recorded, 4 days before and during the measurements, and it is not immediately clear which event lead to the formation of the observed INL. However, Fer et al. (2020) found that bursts of high dissipation rates following a downward displacement of isopycnals persisted only on time scales of hours. Furthermore, restratification after the gravitational collapse of a mixed layer happens within hours (McPhee-Shaw, 2006), and full restratification has not yet occurred at S3. It is, hence likely, that the second event generated the observed strong mixing and consequently the INL above the upper slope.

The observed enhanced velocities might be linked to a larger scale continental shelf wave, resulting from coastal convergences driven by cross-shelf Ekman transport, triggered by the pan-Arctic wind field (Danielson et al., 2020). These waves are propagating eastward along the Arctic shelves, characterized by coastally enhanced sea level anomalies and barotropic disturbances in the flow field, with largest current velocity anomalies near the upper continental slope. The passage of a continental shelf wave and the associated cross-slope barotropic pressure gradient would hence explain the observed enhanced current velocities in both east- and northward direction, but more observational data are needed to confirm this hypothesis. Continental shelf waves were found to be episodic, but re-occurring in the Arctic (Danielson et al., 2020). Based on a 9-year model hindcast, on average 12 surface anomalies linked to CSW were identified per year, with over 60% of these anomalies occurring between August and January (Danielson et al., 2020). This temporal distribution of CSWs roughly resembles the seasonal distribution of the downslope flow events reported here (Figure 3f), which occur exclusively between July and January. Strong barotropic current surges of 0.4–0.5 m s^{-1}, triggered by storms from large scale pressure systems, were also found to cause frequently re-occurring sediment resuspension at the upper slope (water depth of 140–150 m) of the Mackenzie shelf (Forest et al., 2016).

Based on the three year mooring time series (summer 2015 to summer 2018), a total of 23 events with strong current velocity anomalies, a downward flow component >0.15 m s^{-1}, and a contemporaneous drop in potential density >0.15 kg m^{-3} could be identified. These events occur mostly in the second half of the year, between July and October (Figure 3f). Between February and June, no potential mixing events were recorded. This seasonal distribution matches the uneven distribution of continental shelf waves found in Danielson et al. (2020), which are a probable energy source for the enhanced turbulent dissipation rates generating the INL. In addition, likelihood of INL formation varies not only on seasonal, but also inter-annual scale. Both 2015 and 2018 were characterized by a long ice free season and a low minimum sea ice extent (Figure 3f). For those years, the mooring record covers only the freeze-up/melting season, respectively, but still a relatively high number of at least 4/7 events were recorded. In 2016 and 2017, the annual minimum Laptev Sea ice cover extent was larger compared to 2015 and 2018. Only four events were recorded in 2017. In 2016, freeze-up was delayed by approximately 2 weeks (compared to 2017), and eight events were observed. The strong seasonality and interannual variability of potential mixing events toward periods with reduced ice cover in the Laptev Sea suggests that INL formation is closely linked to the absence of sea ice. This supports the hypothesis that their formation is linked to the presence of continental shelf waves. A future reduction of the sea ice cover and elongated ice free periods may result in an increasing number of INLs, and consequently significantly enhanced cross-shelf sediment transport.

The absence of INLs on other transects might be a result of the episodic nature of the flow anomalies that likely caused the INL formation, even though an INL might persist for some time after the event, depending on the settling speed of the suspended particles. The spatially closest transect 125 km upstream of S3 was sampled on September 22. If an INL was formed there during the downslope flow event on September 3 (or a later event), particles had already settled out. However, it is also conceivable that the observed downslope flow at M2 is a spatially confined phenomenon, for example, topographically steered by an incision in the continental slope or a change in direction of the slope orientation, and INLs are hence only generated over a limited along-slope distance. More data are needed to assess both the duration and spatial distribution of INLs along the Laptev Sea continental slope.

4.3. Cross-Slope Transport in the INL

We observed enhanced turbulent mixing which caused sediment resuspension and a turbid layer characterized by a nearly uniform vertical distribution of temperature and salinity, in line with previous INL observations at lower latitudes (e.g., Thorpe & White, 1988). The anticipated subsequent gravitational collapse of this layer will enhance horizontal diffusivities, as the turbid layer spreads laterally along isopycnals (McPhee-Shaw, 2006; McPhee-Shaw et al., 2004; Thorpe & White, 1988). The lateral extent of an INL after the gravitational collapse is in theory bound by the internal Rossby radius $R = \frac{NH}{f}$, where N is the buoyancy frequency, H the vertical length scale (here: 200 m), and f the Coriolis frequency (McPhee-Shaw et al., 2004). Previously reported values for the lateral extent of INLs are in the slightly larger (factor 1.4) than the internal Rossby radius (16 km, continental slope off Porcupine Bank, NE Atlantic Thorpe & White, 1988), or on the order of the internal Rossby radius (3–7 km, northern California margin McPhee-Shaw et al., 2004; McPhee-Shaw, 2006). Depending on the varying background stratification, the local Rossby radius in the Laptev Sea focus region ranges from 2.5 to 7.4 km. Hence, particles transported within the observed INL over the steep slope ($\alpha = 0.15$) can easily reach waters deeper than 1,500 m. The distance between stations S3 and S4 exceeds the size of the local Rossby radius, which might explain the absence of an INL at S4.

From the available data, it is impossible to assess the fraction of PM within the INL that is ultimately exported to the deep basin. Considering 1 mg L^{-1} as a background concentration (see S4, Figure 1a), that is, very fine material with a negligible settling velocity that will not sink out, the integrated concentration of PM above background in the INL at S3 is approximately 500 g m^{-2}. If only 1% of this integrated concentration would be transported toward the basin and subsequently settle at the sea floor, on average eight INL events per year sum up to a total vertical PM flux of 40 g m^{-2} y^{-1}. This value is already higher than the estimated lateral input of lithogenic material to the surface sediments off the Laptev Sea slope (30 g m^{-2} y^{-1}), reported by Fahl and Nöthig (2007) based on sediment trap data from 1995/1996. This bias might indicate that the sedimentation dynamics in the Laptev Sea continental slope region have substantially changed within the last 20 years.

5. Conclusions

Observations from the Laptev Sea provide the first direct evidence of the existence of turbid INLs over continental slopes both polewards of the critical M_2 latitude, and in the Eurasian sector of the Arctic Ocean. The observed turbid layer likely originated from the upper continental slope, at a water depth of 100–200 m. The cloud of PM extended over a vertical range from 60 to 310 m water depth and contained a total PM mass of approximately 650 g m^{-2} and 10 g m^{-2} POC, which is potentially transported toward deeper regions. Locally enhanced turbulent dissipation rates, inducing strong resuspension and vertical mixing, were probably caused by energy release from a trapped lee wave initially developed by isopycnal displacement during intensified (down-slope) current velocities associated with continental shelf waves. More focused observations, including high-resolved time series of water column profiles, are needed to expose the link between continental shelf waves and enhanced mid-water dissipation.

Long-term current velocity data suggests that events potentially leading to an INL formation are re-occurring and take place on average eight times per year, almost exclusively in the ice-free season (July to October), with strong inter-annual variability, probably depending on the sea ice cover. Despite their relatively rare occurrence, INL formation and the associated basin-ward transport of resuspended particles from the upper continental slope may substantially contribute to the cross-slope particle transport and the vertical export of carbon in the Arctic Ocean.

The existence of INLs over the Laptev Sea continental slope emphasizes the close connectivity between the Siberian shelves and the deep Arctic basins. In the future Arctic, increasingly ice-free conditions may reinforce the cross-slope particle transport mechanism investigated in this study. In addition, local sediment supply from dirty sea ice will increase with enhanced melting of first year ice in the marginal ice zone of the Siberian Seas and central Arctic Ocean (Krumpen et al., 2019). With increased shelf sea-ocean coupling, pollutants introduced to the Arctic shelf seas (e.g., by increased marine traffic and the offshore production

of minerals and hydrocarbons) may affect the entire Arctic ecosystem. The discovery of an intermittent off-shelf transport mechanism linked to enhanced turbulent mixing and apparently associated with continental shelf waves is clearly an area requiring further study, particularly as it implies cross-slope particle transport will likely increase with declining sea ice cover.

Data Availability Statement

Figure 1a was produced using the m_map matlab toolbox (Pawlowicz, 2000).

Figure 3a shows wind data from ECMWF Reanalysis v5 (ERA5), produced by the Copernicus Climate Change Service (C3S).

Sea ice data displayed in Figure 3f is available at: Fetterer, F., K. Knowles, W. N. Meier, M. Savoie, and A. K. Windnagel. 2017, updated daily. Sea Ice Index, Version 3. (G02135, Laptev Sea). Boulder, Colorado, USA. NSIDC: National Snow and Ice Data Center. Doi: https://doi.org/10.7265/N5K072F8. Date Accessed: March 15, 2021.

Hydrographic data used in this study were obtained under the framework of the NABOS project with support from NSF (Grants AON-1203473 ans AON-1947162), and are available at:

Igor Polyakov. 2019. Acoustic Dopper Current Profiler (ADCP) from moorings taken in the Eurasian and Makarov basins, Arctic Ocean, 2015–2018. Arctic Data Center. https://doi.org/10.18739/A2HT2GB80; Igor Polyakov and Robert Rember. 2019. Conductivity, Temperature, Pressure (CTD) measurements from Sea Bird Electronics SBE37 instruments taken in the Eurasian and Makarov basins, Arctic Ocean, 2015–2018. Arctic Data Center. https://doi.org/10.18739/A2NK3652R;

Janout, Markus A; Tippenhauer, Sandra; Schulz, Kirstin; Mohrholz, Volker; Ivanov, Vladimir; Polyakov, Igor (2020): Microstructure measurements during Akademik Tryoshnikov cruise AT2018 to the Arctic Ocean. PANGAEA, https://doi.org/10.1594/PANGAEA.925880.

Acknowledgments
The authors would like to thank the crew and participants of the Akademik Tryoshnikov cruise, Igor Polyakov and Ben Möller. Financial support was received from the German Federal Ministry for Science and Education (BMBF) as part of the Changing Arctic Transpolar System (CATS, grant number 03F0776), as well as for the NERC-BMBF-funded PEANUTS-project (grant number 03F0804A and NE/R01275X/1).

References

Azetsu-Scott, K., Johnson, B. D., & Petrie, B. (1995). An intermittent, intermediate nepheloid layer in Emerald Basin, Scotian shelf. *Continental Shelf Research*, *15*(2–3), 281–293. https://doi.org/10.1016/0278-4343(93)E0003-Q

Boetius, A., Albrecht, S., Bakker, K., Bienhold, C., Felden, J., Fernández-Méndez, M., et al. (2013). Export of algal biomass from the melting arctic sea ice. *Science*, *339*(6126), 1430–1432. https://doi.org/10.1126/science.1231346

Cacchione, D. A., & Drake, D. E. (1986). Nepheloid layers and internal waves over continental shelves and slopes. *Geo-Marine Letters*, *6*(3), 147–152. https://doi.org/10.1007/BF02238085

Codiga, D. L. (2011). *Unified tidal analysis and prediction using the UTide Matlab functions*.

Danielson, S. L., Hennon, T. D., Hedstrom, K. S., Pnyushkov, A. V., Polyakov, I. V., Carmack, E., et al. (2020). Oceanic routing of wind-sourced energy along the Arctic continental shelves. *Frontiers in Marine Science*, *7*, 509. https://doi.org/10.3389/fmars.2020.00509

de Madron, X. D., Castaing, P., Nyffeler, F., & Courp, T. (1999). Slope transport of suspended particulate matter on the Aquitanian margin of the Bay of Biscay. *Deep Sea Research Part II: Topical Studies in Oceanography*, *46*(10), 2003–2027. https://doi.org/10.1016/S0967-0645(99)00053-3

de Madron, X. D., Nyffeler, F., & Godet, C. H. (1990). Hydrographic structure and nepheloid spatial distribution in the Gulf of Lions continental margin. *Continental Shelf Research*, *10*(9–11), 915–929. https://doi.org/10.1016/0278-4343(90)90067-V

Dickson, R. R., & McCave, I. N. (1986). Nepheloid layers on the continental slope west of Porcupine bank. *Deep-Sea Research Part A. Oceanographic Research Papers*, *33*(6), 791–818. https://doi.org/10.1016/0198-0149(86)90089-0

Fahl, K., & Nöthig, E.-M. (2007). Lithogenic and biogenic particle fluxes on the Lomonosov Ridge (central Arctic Ocean) and their relevance for sediment accumulation: Vertical vs. lateral transport. *Deep Sea Research Part I: Oceanographic Research Papers*, *54*(8), 1256–1272. https://doi.org/10.1016/j.dsr.2007.04.014

Fer, I., Koenig, Z., Kozlov, I. E., Ostrowski, M., Rippeth, T. P., Padman, L., et al. (2020). Tidally forced lee waves drive turbulent mixing along the arctic ocean margins. *Geophysical Research Letters*, *47*(16), e2020GL088083. https://doi.org/10.1029/2020GL088083

Fer, I., Müller, M., & Peterson, A. K. (2015). Tidal forcing, energetics, and mixing near the Yermak Plateau. *Ocean Science*, *11*, 287–304. https://doi.org/10.5194/os-11-287-2015

Forest, A., Osborne, P. D., Curtiss, G., & Lowings, M. G. (2016). Current surges and seabed erosion near the shelf break in the Canadian Beaufort Sea: A response to wind and ice motion stress. *Journal of Marine Systems*, *160*, 1–16. https://doi.org/10.1016/j.jmarsys.2016.03.008

Forest, A., Osborne, P. D., Fortier, L., Sampei, M., & Lowings, M. G. (2015). Physical forcings and intense shelf-slope fluxes of particulate matter in the halocline waters of the Canadian Beaufort Sea during winter. *Continental Shelf Research*, *101*, 1–21. https://doi.org/10.1016/j.csr.2015.03.009

Forest, A., Sampei, M., Hattori, H., Makabe, R., Sasaki, H., Fukuchi, M., et al. (2007). Particulate organic carbon fluxes on the slope of the Mackenzie Shelf (Beaufort Sea): Physical and biological forcing of shelf-basin exchanges. *Journal of Marine Systems*, *68*(1–2), 39–54. https://doi.org/10.1016/j.jmarsys.2006.10.008

Gardner, W. D., & Walsh, I. D. (1990). Distribution of macroaggregates and fine-grained particles across a continental margin and their potential role in fluxes. *Deep-Sea Research Part A. Oceanographic Research Papers*, *37*(3), 401–411. https://doi.org/10.1016/0198-0149(90)90016-O

Gorsky, G., Ohman, M. D., Picheral, M., Gasparini, S., Stemmann, L., Romagnan, J.-B., et al. (2010). Digital zooplankton image analysis using the ZooScan integrated system. *Journal of Plankton Research*, *32*(3), 285–303. https://doi.org/10.1093/plankt/fbp124

Honjo, S., Krishfield, R. A., Eglinton, T. I., Manganini, S. J., Kemp, J. N., Doherty, K., et al. (2010). Biological pump processes in the cryopelagic and hemipelagic Arctic Ocean: Canada Basin and Chukchi rise. *Progress in Oceanography*, *85*(3–4), 137–170. https://doi.org/10.1016/j.pocean.2010.02.009

Hwang, J., Eglinton, T. I., Krishfield, R. A., Manganini, S. J., & Honjo, S. (2008). Lateral organic carbon supply to the deep Canada Basin. *Geophysical Research Letters*, *35*(11). https://doi.org/10.1029/2008GL034271

Hwang, J., Kim, M., Manganini, S. J., McIntyre, C. P., Haghipour, N., Park, J., et al. (2015). Temporal and spatial variability of particle transport in the deep Arctic Canada Basin. *Journal of Geophysical Research: Oceans*, *120*(4), 2784–2799. https://doi.org/10.1002/2014JC010643

Krumpen, T., Belter, H. J., Boetius, A., Damm, E., Haas, C., Hendricks, S., et al. (2019). Arctic warming interrupts the transpolar drift and affects long-range transport of sea ice and ice-rafted matter. *Scientific Reports*, *9*(1), 1–9. https://doi.org/10.1038/s41598-019-41456-y

McCave, I., & Hall, I. R. (2002). Turbidity of waters over the Northwest Iberian continental margin. *Progress in Oceanography*, *52*(2–4), 299–313. https://doi.org/10.1016/S0079-6611(02)00012-5

McPhee-Shaw, E. (2006). Boundary–interior exchange: Reviewing the idea that internal-wave mixing enhances lateral dispersal near continental margins. *Deep Sea Research Part II: Topical Studies in Oceanography*, *53*(1–2), 42–59. https://doi.org/10.1016/j.dsr2.2005.10.018

McPhee-Shaw, E., Sternberg, R. W., Mullenbach, B., & Ogston, A. S. (2004). Observations of intermediate nepheloid layers on the northern California continental margin. *Continental Shelf Research*, *24*(6), 693–720. https://doi.org/10.1016/j.csr.2004.01.004

Moum, J. N., Caldwell, D. R., Nash, J. D., & Gunderson, G. D. (2002). Observations of boundary mixing over the continental slope. *Journal of Physical Oceanography*, *32*(7), 2113–2130. https://doi.org/10.1175/1520-0485(2002)032⟨2113:OOBMOT⟩2.0.CO;2

O'Brien, M., Macdonald, R., Melling, H., & Iseki, K. (2006). Particle fluxes and geochemistry on the Canadian Beaufort Shelf: Implications for sediment transport and deposition. *Continental Shelf Research*, *26*(1), 41–81. https://doi.org/10.1016/j.csr.2005.09.007

Osborne, P. D., & Forest, A. (2016). Sediment dynamics from coast to slope–southern Canadian Beaufort Sea. *Journal of Coastal Research*, *75*, 537–541. https://doi.org/10.2112/SI75-108.1

Padman, L., Plueddemann, A. J., Muench, R. D., & Pinkel, R. (1992). Diurnal tides near the Yermak Plateau. *Journal of Geophysical Research*, *97*(C8), 12639–12652. https://doi.org/10.1029/92JC01097

Pak, H., Zaneveld, J. R. V., & Kitchen, J. (1980). Intermediate nepheloid layers observed off Oregon and Washington. *Journal of Geophysical Research*, *85*(C11), 6697–6708. https://doi.org/10.1029/JC085iC11p06697

Pawlowicz, R. (2000). *M_Map: A mapping package for Matlab*. University of British Columbia Earth and Ocean Sciences. [Online]. Available: http://www.eos.ubc.ca/rich/map.html

Polyakov, I. V., Rippeth, T. P., Fer, I., Alkire, M. B., Baumann, T. M., Carmack, E. C., et al. (2020). Weakening of cold halocline layer exposes sea ice to oceanic heat in the eastern Arctic Ocean. *Journal of Climate*, *33*(18), 8107–8123. https://doi.org/10.1175/JCLI-D-19-0976.1

Polyakov, I. V., Rippeth, T. P., Fer, I., Baumann, T. M., Carmack, E. C., Ivanov, V. V., et al. (2020). Intensification of near-surface currents and shear in the eastern Arctic Ocean. *Geophysical Research Letters*, *47*(16), e2020GL089469. https://doi.org/10.1029/2020GL089469

Puig, P., Company, J. B., Sardà, F., & Palanques, A. (2001). Responses of deep-water shrimp populations to intermediate nepheloid layer detachments on the Northwestern Mediterranean continental margin. *Deep Sea Research Part I: Oceanographic Research Papers*, *48*(10), 2195–2207. https://doi.org/10.1016/S0967-0637(01)00016-4

Puig, P., & Palanques, A. (1998). Nepheloid structure and hydrographic control on the Barcelona continental margin, northwestern Mediterranean. *Marine Geology*, *149*(1–4), 39–54. https://doi.org/10.1016/S0025-3227(98)00037-1

Rippeth, T. P., Lincoln, B. J., Lenn, Y.-D., Green, J. A. M., Sundfjord, A., & Bacon, S. (2015). Tide-mediated warming of Arctic halocline by Atlantic heat fluxes over rough topography. *Nature Geoscience*, *8*(3), 191–194. https://doi.org/10.1038/ngeo2350

Rippeth, T. P., Vlasenko, V., Stashchuk, N., Scannell, B. D., Green, J. M., Lincoln, B. J., & Bacon, S. (2017). Tidal conversion and mixing poleward of the critical latitude (an Arctic case study). *Geophysical Research Letters*, *44*(24), 12–349. https://doi.org/10.1002/2017GL075310

Schulz, K., Endoh, T., & Umlauf, L. (2017). Slope-induced tidal straining: Analysis of rotational effects. *Journal of Geophysical Research: Oceans*, *122*(3), 2069–2089. https://doi.org/10.1002/2016JC012448

Schulz, K., Janout, M., Lenn, Y.-D., Ruiz-Castillo, E., Polyakov, I., Mohrholz, V., et al. (2021). On the along-slope heat loss of the Boundary Current in the Eastern Arctic Ocean. *Journal of Geophysical Research: Oceans*, *126*(2), e2020JC016375. https://doi.org/10.1029/2020JC016375

Schulz, K., & Umlauf, L. (2016). Residual transport of suspended material by tidal straining near sloping topography. *Journal of Physical Oceanography*, *46*(7), 2083–2102. https://doi.org/10.1175/JPO-D-15-0218.1

Sprent, P. (2012). *Applied nonparametric statistical methods*. Springer Science & Business Media.

Tarasenko, A., Supply, A., Kusse-Tiuz, N., Ivanov, V., Makhotin, M., Tournadre, J., et al. (2021). Properties of surface water masses in the Laptev and the East Siberian seas in summer 2018 from in situ and satellite data. *Ocean Science*, *17*(1), 221–247https://doi.org/10.5194/os-17-221-2021

Thorpe, S., & White, M. (1988). A deep intermediate nepheloid layer. *Deep-Sea Research Part A. Oceanographic Research Papers*, *35*(9), 1665–1671. https://doi.org/10.1016/0198-0149(88)90109-4

van Weering, T. C., De Stigter, H. C., Balzer, W., Epping, E. H., Graf, G., Hall, I. R., et al. (2001). Benthic dynamics and carbon fluxes on the NW European continental margin. *Deep Sea Research Part II: Topical Studies in Oceanography*, *48*(14–15), 3191–3221. https://doi.org/10.1016/S0967-0645(01)00037-6

Wegner, C., Hoelemann, J. A., Dmitrenko, I., Kirillov, S., Tuschling, K., Abramova, E., & Kassens, H. (2003). Suspended particulate matter on the Laptev Sea shelf (Siberian Arctic) during ice-free conditions. *Estuarine, Coastal and Shelf Science*, *57*(1–2), 55–64. https://doi.org/10.1016/S0272-7714(02)00328-1

Xiang, Y., & Lam, P. J. (2020). Size-fractionated compositions of marine suspended particles in the western Arctic Ocean: Lateral and vertical sources. *Journal of Geophysical Research: Oceans*, *125*(8), e2020JC016144. https://doi.org/10.1029/2020JC016144